Highlights

- Fluorophosphoryl diazide and diisocyanate have been synthesized and subsequently characterized by combining IR, Raman, and NMR spectroscopy with quantum chemical calculations.
- The IR spectra of the two phosphoryl compounds reveal the presence of *syn*-*syn* and *anti*-*syn* conformers that differ in the configuration of the two isocyanate ligands with respect to the P=O bond.
- The low-temperature X-ray crystal structure of fluorophosphoryl diisocyanate confirms a favorable *syn*-*syn* conformation.

Graphical abstract:

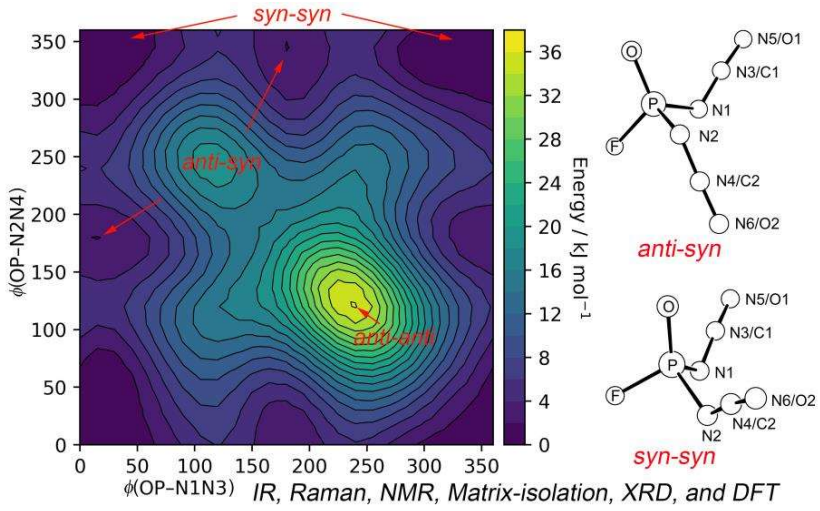

Synthesis and Characterizations of Fluorophosphoryl Diazide and Diisocyanate

Chao Song,[a] Xianxu Chu,[a] Bifeng Zhu,[b] Michael Gerken,[c,*] and Xiaoqing Zeng[a,b,*]

[a] College of Chemistry, Chemical Engineering and Materials Science, Soochow University, 215123 Suzhou, China

[b] Department of Chemistry, Fudan University, Shanghai 200433, China. E-mail: xqzeng@fudan.edu.cn

[c] Canadian Centre for Research in Advanced Fluorine Technologies, University of Lethbridge, 4401 University Drive West, Lethbridge, Alberta T1K 3M4, Canada. E-mail: michael.gerken@uleth.ca

Congratulations to Dr. Robert G. Syvret on receiving the 2020 ACS Award for Creative Work in Fluorine Chemistry

Highlights

- Fluorophosphoryl diazide and diisocyanate have been synthesized and subsequently characterized by combining IR, Raman, and NMR spectroscopy with quantum chemical calculations.
- The IR spectra of the two phosphoryl compounds reveal the presence of *syn*-*syn* and *anti*-*syn* conformers that differ in the configuration of the two isocyanate ligands with respect to the P=O bond.
- The low-temperature X-ray crystal structure of fluorophosphoryl diisocyanate confirms a favorable *syn*-*syn* conformation.

Graphical abstract:

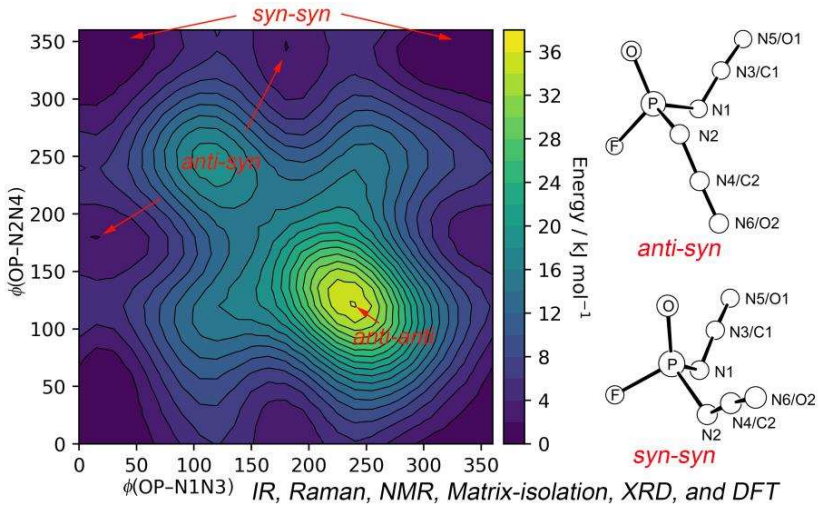

Abstract. Two fluorine-substituted phosphoryl pseudohalides including the highly explosive diazide $FP(O)(N_3)_2$ and diisocyanate $FP(O)(NCO)_2$ have been synthesized and fully characterized with IR (gas-phase and noble-gas matrices), Raman (liquid), and NMR (^{19}F and ^{31}P) spectroscopy. The vibrational spectra of $FP(O)(N_3)_2$ and $FP(O)(NCO)_2$ were analyzed with the aid of the B3LYP/6-311+G(3df) calculations, and the assignments were made in terms of a mixture of *syn-syn* and *anti-syn* conformers, in which the two pseudohalogen groups (N_3 and NCO) adopt *syn*/*anti* configuration to the P=O bond with respect to the P–N bonds. The low-temperature X-ray crystallographic structure of $FP(O)(NCO)_2$ in the solid state reveals C_s molecular symmetry with a *syn-syn* conformation (ϕ(OP–NC) = 54.80(15)°) and weak intermolecular O···C contacts (2.901(2) Å). In line with the experimental observation of dominant *syn-syn* conformers for gaseous $FP(O)(N_3)_2$ and $FP(O)(NCO)_2$, calculations at the CCSD(T)/aug-cc-pVTZ//B3LYP/6-311+G(3df) level demonstrate that the *anti-syn* conformers are higher in energy (ΔG) by 3.8 and 3.2 kJ mol^{-1}, respectively.

Keywords: azides, isocyanates, phosphoryl fluorides, conformation, vibrational spectroscopy

Introduction

Covalent azides are versatile reagents in synthetic chemistry such as the construction of heterocyles through click-reactions and the nitrogenation of C-H bonds via the intermediacy of transient nitrenes.[1–3] Generally, azides are energetic and sometimes highly explosive due to exothermic fragmentation by eliminating molecular nitrogen upon heating or irradiation. Hence, the synthesis, isolation, and characterization of azides especially polyazides that contain more than one azide ligand in the molecule are challenging. In the past two decades, a growing number of polyazides of group 14 elements (C, Si),[4–6] 15 (P, As, Sb, Bi),[7–10] and 16 (S, Se, Te)[10–16] have been isolated and structurally characterized, although some of these explosive compounds may have already been known in solutions for some time. Among these main-group elements, phosphorus shows rich coordination chemistry, and hence a number of highly energetic phosphorus-centered azides have been synthesized including binary compounds (e.g., $P(N_3)_3$, $P(N_3)_5$, $[P(N_3)_4]^+$, and $[P(N_3)_6]^-$)[17] and derivatives containing trivalent phosphorus P(III) such as F_2PN_3,[18,19] $CH_3OP(N_3)_2$,[20] and $Ph_2NP(N_3)_2$.[21] Such compounds have been used as molecular precursors for the generation of highly reactive low-valent phosphorus compounds such as phosphinonitrenes[22,23] and phosphinidenes[20,24] through N_2-elimination.

By analogy, the structures and reactivity of phosphoryl azides have also attracted interest in phosphorus chemistry. For example, difluorophosphoryl azide ($F_2P(O)N_3$) adopts an approximate C_s symmetry with *cis*-conformation between the P=O bond and the N_3 moiety in the gas phase and solid state,[25,26] and its decomposition yields a thermally persistent triplet phosphoryl nitrene ($F_2P(O)N$) in the gas phase.[27] The formation of rigid phosphoryl nitrene has also been observed in the photodecomposition of diphenylphosphoryl azide in solution.[28,29] In contrast to the nitrene formation in the fragmentation of phosphoryl monoazide ($R_2P(O)N_3$), the complete decomposition of phosphoryl diazides ($RP(O)(N_3)_2$, R = F,[30] CH_3[20] and Ph[31]) provides an unique access to phosphinidene oxides (RPO), which are not only useful ligands in coordination chemistry[32] but also serve as key intermediates in the combustion and degradation of phosphorus-based flame retardants in the atmosphere.[33] When compared to the monoazide, the higher energy content in diazides renders their characterization more challenging. To the best of our knowledge, none of the aforementioned phosphoryl diazides have been structurally characterized. As for the triazide $OP(N_3)_3$, it acts as an ideal precursor for the linear triatomic molecule OPN,[34] which is a heavy congener of nitrous oxide (N_2O) that can combine with CO to form quasilinear OPNCO molecule.[35] Despite of being exceedingly explosive, $OP(N_3)_3$ and its sulfur analog $SP(N_3)_3$ have already been fully characterized as a neat substances.[36]

Structurally, the thermally more robust isocyanates are close analogues of azides. As important reagents for the synthesis of biologically active heterocycles[37,38] and polyurethane materials in industry,[39] covalent isocyanates display similar structural and conformational properties as azides.[25] For instance, both carbonyl diisocyanate ($OC(NCO)_2$)[40,41] and diazide ($OC(N_3)_2$)[5,42] are planar and exist as mixtures of *syn-syn* and *syn-anti* conformers in the gas phase, whereas only the lower-energy *syn-syn* conformer was found for both compounds in the solid state. Similar to the stepwise decomposition of $OC(N_3)_2$ (→ $OC(N_3)N$ → $OCN–N_3$ → CO + 2 N_2),[43] the photolysis of $OC(NCO)_2$ in a cryogenic Ar-matrix results in CO-elimination and yields the carbonyl nitrene OC(NCO)N followed by rearrangement to diisocyanate OCNNCO.[44,45] The latter undergoes further fragmentation to CO and N_2 via the intermediacy of the putative nitrene intermediate NNCO.[46] The similar decomposition reactions for azides and isocyanates also stimulate the recent study on the parent alkynyl isocyanate HCCNCO,[37] whose decomposition provides an alternative method for the generation of cyanocarbene HCCN,[47] an important intermediate in the interstellar medium that was previously generated from the decomposition of the highly explosive diazoacetonitrile ($HC(N_2)CN$)[48] or alkynyl azide ($HCCN_3$).[49] In addition to the decomposition reactions, the structures of binary isocyanates ($B(NCO)_3$,[50] $Si(NCO)_4$,[51] and $S(NCO)_2$[52]) and various derivatives including phosphorus(III) isocyanates such as $P(NCO)_3$,[53] F_2PNCO,[54] Cl_2PNCO [55] have also been reported. For phosphorus(V) isocyanates, the structures of both $F_2P(O)NCO$[25] and $F_2P(S)NCO$[56] have been determined. The triisocyanate $OP(NCO)_3$ has also been characterized in solution,[57] however, phosphoryl diisocyanates including $FP(O)(NCO)_2$ remain yet undocumented.

Continuing the increasing interest in the structures and reactivity of phosphorus-containing azides,[5,10-12,18,21,25,36] herein, we report the synthesis and characterization of phosphoryl diazide $FP(O)(N_3)_2$ and the closely related diisocyanate $FP(O)(NCO)_2$ from both aspects of experiment and theory. Prior to this study, only the diazide $FP(O)(N_3)_2$ has been previously characterized by ^{19}F and ^{31}P NMR spectroscopy in solution.[58]

Experimental Section

Caution! Covalent azides are in general explosive. Although no explosions were encountered with $FP(O)(N_3)_2$ during this work, it should be handled with care in small quantities (< 5 mmol) and appropriate safety precautions should be taken.

General Procedure and Reagents: Volatile materials were manipulated in a glass vacuum line

equipped with three U-traps and valves with PTFE stems (Young, London, UK). The vacuum line was connected to an IR gas cell (optical path length 20 cm, Si windows, 0.6 cm thick) contained in the sample compartment of the FT-IR instrument (Bruker, Tensor 27), which was used for IR spectroscopic characterization of volatile products. The final products were stored in flame-sealed glass ampoules in liquid nitrogen. The starting material $FP(O)Cl_2$[59] was synthesized according to the literature protocol. NMR spectra were measured in CD_2Cl_2 solutions at room temperature on a Bruker Avance 400 spectrometer: ^{19}F NMR (376.5 MHz), ^{31}P NMR (242.9 MHz), and ^{14}N NMR (43.4 MHz). The chemical shifts are referenced to external $CFCl_3$ (^{19}F), H_3PO_4 (^{31}P), and CD_3NO_2 (^{14}N).

Synthesis of $FP(O)(N_3)_2$: Fluorophosphoryl diazide was prepared by reacting $FP(O)Cl_2$ (70 mg, 0.5 mmol) with NaN_3 (0.2 g, 3 mmol) in CH_3CN (1 mL) at room temperature.[30] Traces of byproduct $OP(N_3)_3$ can be removed by passing the volatile products through a cold trap at –20 ºC. The more volatile $FP(O)(N_3)_2$ (45 mg, 0.3 mmol) is retained in a cold trap –60 ºC. The purity was ascertained by NMR spectroscopy: ^{19}F NMR: δ = –59.7 ppm (d, $^1J(^{31}P–^{19}F)$ = 1032 Hz); ^{31}P NMR: δ = –4.6 ppm (d). ^{14}N NMR: $\delta(N_\alpha)$ = –297.5 ppm (s, $\Delta\nu_{½}$ = 413.0 Hz), $\delta(N_\beta)$ = –152.2 ppm (s, $\Delta\nu_{½}$ = 16.2 Hz), $\delta(N_\gamma)$ = –163.0 ppm (s, $\Delta\nu_{½}$ = 54.5 Hz).

Synthesis of $FP(O)(NCO)_2$: Fluorophosphoryl diisocyanate was prepared by reacting $FP(O)Cl_2$ (1.4 g, 10 mmol) with dried AgOCN (4.0 g, 27 mmol) in CH_3CN (3 mL) at room temperature (24 hours). The volatile products were separated by fractional condensation. After passing through a –5 ºC trap, $FP(O)(NCO)_2$ (1.05 g, 7.0 mmol) was retained in a trap at –45 ºC as white solid, traces of F_3PO were identified in the –196 ºC trap. The purity was ascertained by NMR spectroscopy: ^{19}F NMR: δ = –53.9 ppm (d, $^1J(^{31}P–^{19}F)$ = 949 Hz); ^{31}P NMR: δ = –32.8 ppm (d).

Raman Spectroscopy. Raman spectra of liquids were recorded with a Bruker-Equinox 55 FRA 106/S FT-Raman spectrometer using an Nd:YAG laser (200 mW), 200 scans were averaged at a resolution of 2 cm^{-1}. Liquid samples were flame-sealed in 4-mm glass capillaries for the measurement.

Matrix-isolation IR spectroscopy. Gaseous $FP(O)(N_3)_2$ was mixed with argon (1:1000) in a 1 L stainless-steel storage container and then small amounts (ca. 1 mmol) of the mixture were deposited in 30 minutes onto the cold matrix support (16 K, Rh plated Cu block) in high vacuum. Matrix IR spectra were recorded on a FT-IR spectrometer (Bruker 70V) in reflectance mode using a transfer optic. A KBr beam splitter and an MCT detector were used in the region of 4000 to 550 cm^{-1}. For each spectrum, 200 scans at a resolution of 0.5 cm^{-1} were co-added.

Crystal Growth of $FP(O)(NCO)_2$: Crystals of $FP(O)(NCO)_2$ were grown in an L-shaped glass

tube (o.d. 0.6 cm, length 20 cm). Small amounts (ca. 20 mg) of the compound were condensed into the upper part of the L-tube at –196 °C, which was connected to the vacuum line and subsequently flame-sealed. For crystallization, the end without sample was immersed into an ethanol cold bath at –20 °C, while the end with sample was kept in an ice-water bath. Under these conditions, needles grew at the colder end of the tube after 4 h. Then, the tube containing the crystals was cut in a cold nitrogen stream (ca. –70 °C), and the crystals were quickly transferred into a trough cooled by a flow of cold nitrogen and mounted. A crystal of $FP(O)(NCO)_2$ having the dimensions 0.374 × 0.064 × 0.038 mm^3 was selected at ca. –70 °C under the microscope. Attempts to grow crystals of $FP(O)(N_3)_2$ in a similar manner failed, only a supercooled liquid was observed even at –78 °C.

X-ray Crystallography Diffraction: Crystals were centered on an Oxford Diffraction Gemini E Ultra diffractometer, equipped with a 2K × 2K EOS CCD area detector, a four-circle kappa goniometer, an Oxford Instruments Cryojet, and sealed-tube Enhanced (Mo) and the Enhanced Ultra (Cu) sources. For the data collection the Mo source emitting graphite-monochromated Mo-Kα radiation (λ = 0.71073 Å) was used. The diffractometer was controlled by the CrysAlis^{Pro} Graphical User Interface (GUI) software.[60] The diffraction data collection strategy was optimized with respect to complete coverage and consisted of two ω scans with a width of 1°. The data collection for $FP(O)(NCO)_2$ was carried out at −123 °C in a 1024 x 1024 pixel mode using 2 × 2 pixel binning. Processing of the raw data, scaling of diffraction data and the application of an empirical absorption correction was completed by using the CrysAlis^{Pro} program.[61] Atom positions were determined using the intrinsic phasing method (ShelXT) [62] and were refined using least-squares refinement (ShelXL).[63] The final refinement was obtained by introducing anisotropic thermal parameters and the recommended weightings for all of the atoms (Table 1). Structure solution and refinement were performed with the aid of Olex2 (version 1.2). [64] CCDC 2039718 contains the supplementary crystallographic data for this paper. These data can be obtained free of charge from the Cambridge Crystallographic Data Centre (CCDC) via http://www.ccdc. cam.ac.uk/data_request/cif.

Table 1. Summary of crystallographic data for $FP(O)(NCO)_2$.

chemical formula	$C_2FN_2O_2P$
M_r	150.01
crystal system	orthorhombic
space group	*Pnma*
a (Å)	5.3036(4)
b (Å)	11.6941(11)
c (Å)	8.1033(7)
α (deg)	90
β (deg)	90
γ (deg)	90
V(Å^3)	502.57(7)
Z (molecules/unit cell)	4
mol wt	150.01
calculated density (g cm^{-3})	1.985
T (K)	150
μ (mm^{-1})	0.494
R_1[a]	0.0331
wR_2[b]	0.0820

[a] R_1 is defined as $\Sigma||F_o| - |F_c||/\Sigma|F_o|$ for $I > 2\sigma(I)$. [b] wR_2 is defined as $[\Sigma w(F_o^2 - F_c^2)^2/\Sigma w(F_o^2)^2]^{1/2}$ for $I > 2\sigma(I)$.

Computational Details: Geometry optimizations with the DFT (B3LYP,[65] BP86,[66] mPW1PW91[67]) methods were performed and the 6-311+G(3df) basis set using the Gaussian 09 software package.[68] Single point energies at CCSD(T)/aug-cc-pVTZ[69] level were carried out based on the B3LYP/6-311+G(3df) optimized structures with the MOLPRO 2015 program.[70] Relaxed potential energy scans were performed at the B3LYP/6-311+G(d) level by optimizing the structures while rotating the dihedral angles around the two P−N bonds.

Results and Discussion

Physical Properties of $FP(O)X_2$ (X = N_3, NCO)

Both phosphoryl compounds $FP(O)X_2$ (X = N_3, NCO) can be stored in CH_3CN without noticeable decomposition for weeks at room temperature. As for the pure substances, slow ligand exchange happens with the formation of OPF_3 and less volatile $OP(N_3)_3$ and $OP(NCO)_3$, respectively. The diazide $FP(O)(N_3)_2$ is a colorless liquid that has a vapor pressure of ca. 3 mbar at 25 ºC, allowing the transfer of the substance on the vacuum line. When slowly freezing the liquid azide to –196 ºC, it becomes glassy solid that changes to a supercooled liquid at around –78 °C. In contrast, $FP(O)(NCO)_2$ is a white solid at –78 °C and it has a sharp melting point of 19.8 ºC with a vapor pressure of ca. 2 mbar at room temperature.

Quantum Chemical Calculations

The molecular structures of $FP(O)X_2$ (X = N_3, NCO) were optimized with different DFT methods (B3LYP, BP86, and mPW1PW91) using the 6-311+G(3df) basis set. For both species, two conformers (*anti-syn* and *syn-syn*), differing in the configuration (*syn* and *anti*) of the two pseudohalogen ligands X with respect to the P=O bond, are true minima on the potential energy surface (Figure 1). However, a third conformer containing the sole *anti*-conformations between X and the P=O bond (*anti-anti*) is unstable and relaxes to the *anti-syn* conformation by spontaneous rotation around the P−N bond. The calculated conformational properties of $FP(O)X_2$ (X = N_3, NCO) are quite similar to those of the triazide $OP(N_3)_3$, for which only two conformers of *syn-syn-syn* and *syn-anti-syn* with C_3 and C_s symmetries are stable.[36] In contrast, the replacement of the phosphoryl oxygen atom by lone-pair electrons leads to three minima for $P(N_3)_3$, and the calculated global minimum is the *syn-anti-syn* conformer in which only one N_3 group adopts the *anti*-conformation with respect to the lone-pair electrons at the phosphorus atom.[71] For the heavy congener $As(N_3)_3$, the *anti-syn-anti* conformer is most stable in the gas phase, however, its X-ray crystal structure in the solid state reveals a distorted C_3 structure with all the three N_3 ligands in an *anti*-configuration to the lone-pair electrons at the central As atom.[72]

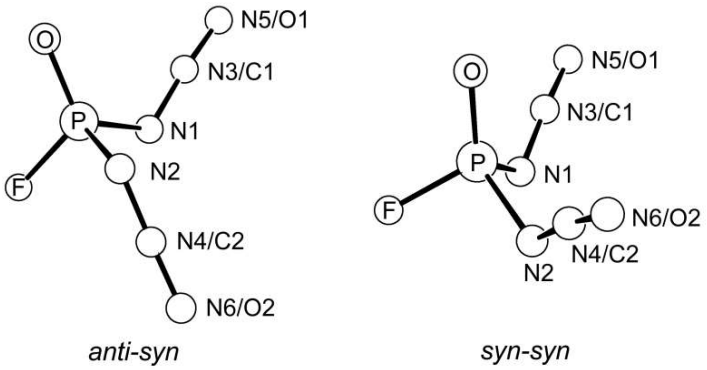

Figure 1. Two stable conformers of $FP(O)X_2$ (X = N_3, NCO).

For both $FP(O)(N_3)_2$ and $FP(O)(NCO)_2$, all the applied theoretical methods conclusively suggest that the *syn-syn* conformer is more stable than the *anti-syn* conformer (Table 2). Specifically, the *syn-syn* conformer of $FP(O)(N_3)_2$ is lower by 3.8 kJ mol^{-1} at the CCSD(T)/aug-cc-pVTZ//B3LYP/6-311+G(3df) level of theory, corresponding to an equilibrium abundance of 17.7% for the less stable *anti-syn* conformer at 298K. By analogy, an abundance of 21.6% at equilibrium for the *anti-syn* conformer of $FP(O)(NCO)_2$ should render its observation possible under ambient conditions. The preference of a *syn*-conformation between the

pseudohalogen ligand and the P=O bond has also been computationally predicted for $F_2P(O)N_3$ and $F_2P(O)NCO$ and also experimentally verified with their crystal structures, and the bonding analysis results indicated the dominance of electronic stabilizing hyperconjugation (anomeric effect) of the lone-pair electrons at the bridging nitrogen atom (N_α) to the anti-bonding P=O orbital ($n_\sigma(N_\alpha) \rightarrow \sigma^*(P=O)$).[25] Similar intramolecular donor-acceptor interaction has also been found for other phosphates,[73] sulfates,[74] and sulfinates.[75]

Table 2. Calculated relative total energies (ΔE, kJ mol^{-1}), Gibbs free energies (ΔG, kJ mol^{-1}), and the predicted equilibrium abundances ratios for the *anti-syn* conformers of $FP(O)X_2$ (X = N_3 and NCO) at 298 K.

methods	$FP(O)(N_3)_2$			$FP(O)(NCO)_2$		
	ΔE	ΔG	% *anti-syn*	ΔE	ΔG	% *anti-syn*
B3LYP [a]	2.3	3.6	19.0	5.2	2.9	23.7
BP86 [a]	1.7	3.7	18.3	5.1	3.6	19.0
mPW1PW91 [a]	2.4	3.8	17.7	5.2	3.3	20.9
CCSD(T)[b]	2.5	3.8	17.7	5.5	3.2	21.6

[a] At the 6-311+G(3df) basis set. [b] Single-point energies at the aug-cc-pVTZ basis set based on the B3LYP/6-311+G(3df) calculated structures.

To probe the underlying mechanism for the conformational interconversion, the potential energy profile for the rotation of the two P–N bonds in $FP(O)(N_3)_2$ was calculated at the B3LYP/6-311+G(d) level by scanning the corresponding two dihedral angles (Figure 2). The *anti-anti* conformer is higher than the *anti-syn* conformer by more than 30 kJ mol^{-1}. The *syn-syn* → *anti-syn* conversion by rotating the P–N bond needs to overcome a small barrier of 6 kJ mol^{-1}, which is comparable with the same conformational transformation in $FP(O)(NCO)_2$ (5 kJ mol^{-1}, Figure S1 in the Supporting Information). For both species, the barriers for the reverse conformational conversion are even lower (3.8 kJ mol^{-1} for $FP(O)(N_3)_2$ and 0.02 kJ mol^{-1} for $FP(O)(NCO)_2$). The similarity in energies and the associated small barriers for the two stable conformers of the azide and isocyanate imply the facile conformational conversion at ambient conditions.

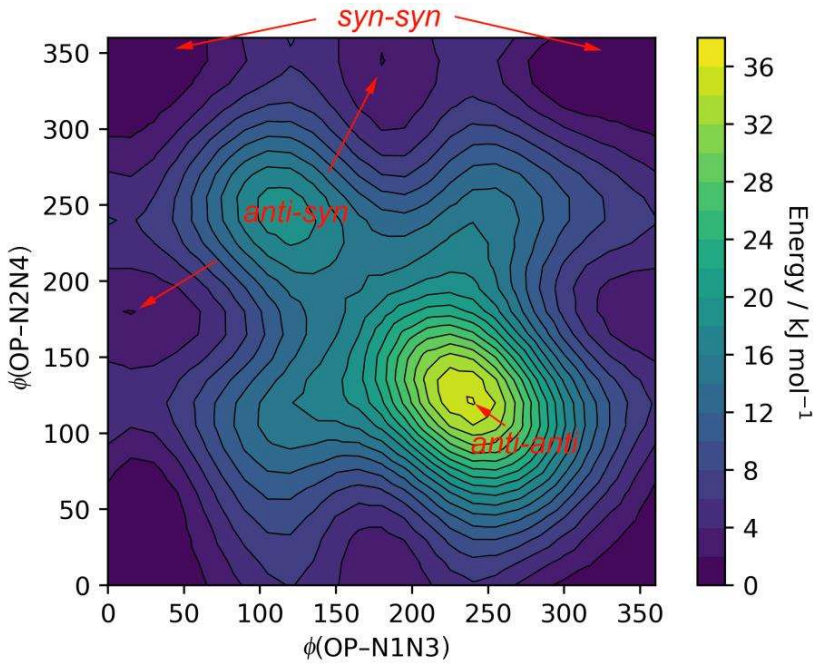

Figure 2. Calculated potential energy profile for the rotation of the P–N bonds in $FP(O)(N_3)_2$ at the B3LYP/6-311+G(d) level.

Vibrational Spectra of $FP(O)(N_3)_2$

The IR (gas-phase and Ar-matrix) and Raman (liquid) spectra of $FP(O)(N_3)_2$ are shown in Figure 3. The vibrational frequencies are listed in Table 3 together with the B3LYP/6-311+G(3df) calculated frequencies of the *anti-syn* and *syn-syn* conformers.

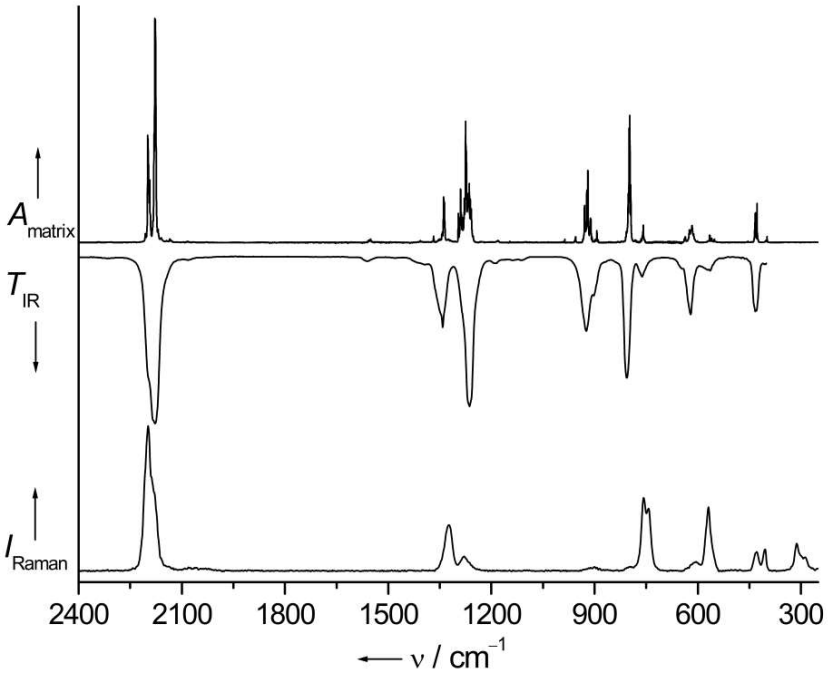

Figure 3. Ar-matrix IR (upper trace, absorbance *A*, resolution 0.25 cm^{-1}, 16 K), gas-phase IR (middle trace, transmission *T*, resolution 2 cm^{-1}, 300 K), and liquid Raman (lower trace, Raman

intensity *I*, resolution 2 cm^{-1}, 300 K) spectra of $FP(O)(N_3)_2$.

The strongest broad band in the gas-phase IR spectrum of $FP(O)(N_3)_2$ (Figure 3, middle trace) at 2178 cm^{-1} belongs to the N_3 asymmetric stretches. It splits into two well-resolved bands at 2199.5 and 2178.3 cm^{-1} in the Ar-matrix IR spectrum (Figure 2, upper trace), corresponding to the in-phase and out-of-phase combinations of the asymmetric stretches of the two azide groups. The band positions (2199.5/2178.3 cm^{-1}) are right between the frequencies for the N_3 asymmetric stretches in $F_2P(O)N_3$ (2206.2 cm^{-1}, Ar-matrix)[25] and $OP(N_3)_3$ (2190.0/2172.4 cm^{-1}, Ar-matrix).[36] The P=O stretching mode in the Raman spectrum of liquid $FP(O)(N_3)_2$ is located at 1323 cm^{-1}, which is red-sifted comparing with those observed in the gas phase (1341 cm^{-1}) and the Ar-matrix (1338.7 cm^{-1}), implying the possible intermolecular interactions in the condense phase. A similar red-shift in the P=O stretching frequencies was observed for $OP(N_3)_3$, in which the oxygen atoms interact with the central nitrogen atom (N_β) through a distance of 2.875 Å in the solid-state. The observed P=O stretching frequency in $FP(O)(N_3)_2$ (1341 cm^{-1}) is lower than those in $F_2P(O)N_3$ (1377 cm^{-1}) and F_3PO (1415 cm^{-1}), but it is higher than that in $OP(N_3)_3$ (1301 cm^{-1}),[36] which is fully consistent with the relationship between the P=O stretching frequency and the electronegativity of the substituent in these phosphoryl compounds. The consecutive substitution of fluoride with azide results in a decrease of the P=O stretching frequency by 36 to 40 cm^{-1} per azide group.

Table 3. Experimental and calculated vibrational frequencies (cm^{-1}) of $FP(O)(N_3)_2$

experimental			calculated (IR) [Raman][d]		assignment[e]
IR gas-phase[a]	Ar-matrix[b]	Raman liquid[c]	*anti-syn*	*syn-syn*	*syn-syn*
2198 sh	2199.5 s	2198 vs	2313 (336) [127]	2317 (352) [109]	$\nu_{as}(N_3)$, in-phase
2178 vs	2178.3 vs	2179 sh	2292 (860) [52]	2299 (853) [65]	$\nu_{as}(N_3)$, out-of-phase
1341 s	1338.7 s	1323 s	1372 (253) [21]	1374 (133) [16]	ν(PO)
1264 vs	1274.9 vs	1279 w	1340 (205) [3]	1342 (480) [2]	$\nu_s(N_3)$, in-phase
			1338 (392) [2]	1325 (178) [5]	$\nu_s(N_3)$, out-of-phase
924 s	929.3 s	911.4 vw		900 (230) [2]	ν(PF)
901 sh	910.7 m		878 (210) [1]		$\nu(PF)_{anti\text{-}syn}$
807 s	797.6 s	796 w	791 (253) [1]	788 (300) [1]	ν_{as}(NPN)
762 m	758.9 m	758 s	731 (20) [11]	747 (42) [11]	ν_s(NPN)
621 s	617.0 m	608 w	623 (131) [2]	632 (121) [3]	$\delta_{i.p.}(N_3)$, out-of-phase
			590 (3) [1]	585 (8) [< 1]	$\delta_{o.o.p.}(N_3)$, in-phase
564 w	565.9 w	569 s	583 (26) [13]	579 (9) [3]	$\delta_{i.p.}(N_3)$, in-phase
	552.0 vw		580 (9) [1]	575 (13) [11]	$\delta_{o.o.p.}(N_3)$, out-of-phase
432 m	432.2 m		432 (37) [1]	429 (52) [1]	
429 m	427.9 m	429 m	418 (33) [1]	428 (28) [1]	
405 w	398.6 w	405 m	399 (16) [2]	393 (8) [2]	
	313.3 vw	313 m	304 (< 1) [2]	304 (1) [2]	

	288 w	288 (< 1) [2]	276 (< 1) [1]

[a] Observed frequencies in the gas phase (300 K) with relative band intensities: vs very strong, s strong, m medium strong, w weak, vw very weak, and sh shoulder. [b] The band positions of the most intense matrix sites (16 K). [c] Observed frequencies in the liquid state (300 K). [d] B3LYP/6-311+G(3df) level of theory; IR intensities (km mol^{-1}) in parentheses and Raman intensities ($Å^4$ u^{-1}) in square brackets, calculated frequencies below 250 cm^{-1} are not listed. [e] Assignments were made according to the calculated vibration displacement vectors of the *syn-syn* conformer.

According to the calculations at the B3LYP/6-311+G(3df) level (Table 3), the IR spectra for the two conformers of $FP(O)(N_3)_2$ are predicted to be very similar, including the two P=O stretching vibrations at 1372 and 1374 cm^{-1} for the *anti-syn* and *syn-syn* conformers, respectively. However, the P–F stretching frequencies in the two conformers (*anti-syn*: 878 cm^{-1}; *syn-syn*: 900 cm^{-1}) differ by 22 cm^{-1} (Table 3). Indeed, the strong band at 924 cm^{-1} in the IR spectrum of gaseous $FP(O)(N_3)_2$ displays a shoulder at 901 cm^{-1} (Figure 3, middle trace), which very likely belongs to the less stable *anti-syn* conformer. According to the observed and calculated IR intensities of these two bands, a ratio of 16.6% for the *anti-syn* conformer at room temperature (300 K) was estimated, it is in good agreement with the calculated ratio of 18% at the CCSD(T)/aug-cc-pVTZ//B3LYP/6-311+G(3df) level of theory (Table 2). In the Ar-matrix IR spectrum (Figure 3, upper trace), two main bands at 929.3 and 910.7 cm^{-1} with additional satellite bands due to different matrix sites were observed, and similar splittings were also found for the bands of the NPN stretching and N_3 deformation modes.

Vibrational Spectra of $FP(O)(NCO)_2$

The IR (gas-phase and Ne-matrix) and Raman (liquid) spectra of $FP(O)(NCO)_2$ are shown in Figure 4. The experimental and the B3LYP/6-311+G(3df) calculated vibrational frequencies are listed in Table 4.

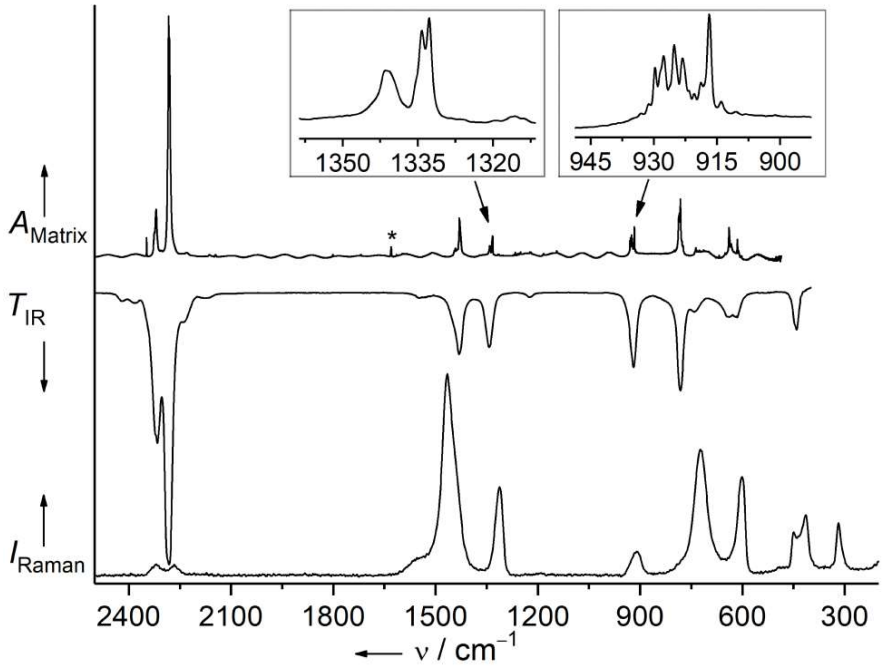

Figure 4. Ne-matrix IR (upper trace, absorbance *A*, resolution 0.25 cm^{-1}, 2.8 K), gas-phase IR (middle trace, transmission *T*, resolution 2 cm^{-1}, 300 K), and liquid Raman (lower trace, Raman intensity *I*, resolution 2 cm^{-1}, 300 K) spectra of $FP(O)(NCO)_2$. The band for H_2O is labeled with an asterisk.

Two well-resolved strong bands at 2316 and 2282 cm^{-1} in the gas-phase IR spectrum (Figure 4, middle trace) occur for the in-phase and out-of-phase combinations of the NCO asymmetric stretches, and the band positions slight shift to 2319.8 and 2283.3 cm^{-1} in the Ne-matrix (Figure 3, upper trace). In the liquid state, they appear as two very weak bands at 2320 and 2266 cm^{-1} in the complementary Raman spectrum (Figure 4, lower trace). The two NCO symmetric stretches appear at 1456/1432 and 1441.8/1430.3 cm^{-1} in the IR spectra for the gaseous and Ne-matrix isolated $FP(O)(NCO)_2$. The P=O stretching frequency (gas-phase IR: 1344 cm^{-1}, Raman: 1313 cm^{-1}) is very close to that of $FP(O)(N_3)_2$ (gas-phase IR: 1341 cm^{-1}, Raman 1323 cm^{-1}), and the noticeable shift of 31 cm^{-1} for the band positions observed in the gas phase and liquid suggests the presence of weak intermolecular interactions of the P=O moiety. According to the calculated IR spectra for $FP(O)(NCO)_2$, the P=O stretching mode in the less stable *anti-syn* conformer (1353 cm^{-1}) is higher in frequency than the *syn-syn* conformer (1338 cm^{-1}) by 15 cm^{-1}. In line with the theoretical prediction, there are two bands at 1341.2 and 1332.7 cm^{-1} in the IR spectrum of Ne-matrix isolated $FP(O)(NCO)_2$ (Figure 4, inset), corresponding to the *anti-syn* and *syn-syn* conformers, respectively. As a further proof, two sets of bands centered at 925.1 and 916.9 cm^{-1} appear in the spectrum for the *anti-syn* and *syn-syn* conformers with calculated frequencies of 889

and 880 cm^{-1} (Table 4). Based on the intensities of the two IR bands for the P=O stretching vibrations, an abundance of 29.1% for the higher-energy *anti-syn* conformer in Ne-matrix was estimated. The presence of two conformers in Ne-matrix indicates their existence also in the gas phase at room temperature; however, their bands in the corresponding gas-phase IR spectrum strongly overlap (Figure 4, middle trace).

Table 4. Experimental and calculated vibrational frequencies (cm^{-1}) of $FP(O)(NCO)_2$

experimental				calculated (IR) [Raman][e]		assignment[f]
IR		Raman		*anti-syn*	*syn-syn*	*syn-syn*
gas-phase[a]	Ne-matrix[b]	liquid[c]	solid[d]			
2316 s	2319.8 s	2320 w	2301 vw	2394 (700) [3]	2394 (426) [5]	ν_{as}(NCO), in-phase
2282 vs	2283.3 vs	2266 w	2261 vw	2353 (2248) [4]	2354 (2632) [4]	ν_{as}(NCO), out-of-phase
1456 w	1441.8 w	1466 vs	1472 vs	1502 (123) [42]	1497 (51) [55]	ν_{s}(NCO), in-phase
1432 s	1430.3 s			1477 (157) [19]	1479 (220) [6]	ν_{s}(NCO), out-of-phase
	1341.2 s			1353 (207) [11]		ν(PO)$_{anti\text{-}syn}$
1344 s	1332.7 s	1313 s	1301 s		1338 (178) [10]	ν(PO)
919 s	925.1 s	911 m	929 m		889 (228) [3]	ν(PF)
	916.9 s			880 (221) [3]		ν(PF)$_{anti\text{-}syn}$
783 s	786.0 s	776 sh			765 (385) [1]	ν_{as}(NPN)
	781.9 s			760 (357) [1]		ν_{as}(NPN)$_{anti\text{-}syn}$
742 w	736.8 w	725 s	711 s		718 (96) [10]	ν_{s}(NPN)
	726.0 w			699 (78) [9]		ν_{s}(NPN)$_{anti\text{-}syn}$
640 m	639.4 m				643 (101) [1]	$\delta_{i.p.}$(NCO), out-of-phase
	632.9 m			636 (88) [1]		$\delta_{i.p.}$(NCO)$_{anti\text{-}syn}$, out-of-phase
618 m	614.7 m		606 w	625 (38) [< 1]	623 (45) [< 1]	$\delta_{o.o.p.}$(NCO), in-phase
		602 s	593 s	620 (13) [< 1]	619 (5) [< 1]	$\delta_{o.o.p.}$(NCO), out-in-phase
				605 (20) [9]	604 (10) [10]	$\delta_{i.p.}$(NCO), in-phase
441 m		450 m	450 s	443 (53) [1]	440 (29) [1]	
		414 s	419 s	423 (36) [2]	436 (72) [1]	
		319 s	321 m	403 (19) [2]	389 (9) [3]	
				306 (0.2) [2]	307 (0.1) [< 1]	
				302 (0.7) [1]	296 (0.8) [1]	

[a] Observed frequencies in the gas phase (300 K) with relative band intensities: vs very strong, s strong, m medium strong, w weak, vw very weak, and sh shoulder. [b] The band positions of the most intense matrix sites (2.8 K). [c] Observed frequencies in the liquid state (300 K). [d] Observed frequencies in the solid state (77 K). [e] B3LYP/6-311+G(3df) level of theory; IR intensities (km mol^{-1}) in parentheses and Raman intensities ($Å^4$ u^{-1}) in square brackets, calculated frequencies below 250 cm^{-1} are not listed. [f] Assignments were made according to the calculated vibration displacement vectors of the *syn-syn* conformer.

Crystal Structure of $FP(O)(NCO)_2$

Colorless needle crystals of $FP(O)(NCO)_2$ can be grown by slow sublimation of the solid compound (0 °C) in one end of a flame-sealed glass tube to another end of the tube at –20 °C. The diisocyanate crystallizes in the *Pnma* space group with four molecules in the unit cell. The crystal

structure of $FP(O)(NCO)_2$ is shown in Figure 5, and the refined structural parameters are given in Table 5 together with the B3LYP/6-311+G(3df) calculated data.

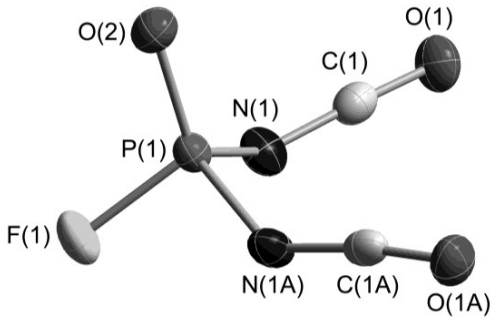

Figure 5. Molecular structure of $FP(O)(NCO)_2$ with thermal ellipsoids at the 50% probability level.

Comparing to the two optimized conformers in Figure 1, the crystal structure of solid $FP(O)(NCO)_2$ represents the energetically more stable *syn-syn* conformer with C_s symmetry. In general, the experimental bond lengths and angles show good agreement with the calculations (Table 5), but the two isocyanate groups are strongly distorted from the OPN plane with dihedral angles of ϕ(OP–N1C1) = 54.80(15)º, which are significantly larger than the calculated value of –5.8º. This discrepancy is probably due to intermolecular interactions in the solid state (Figure 6).

Table 5. Calculated and experimental structural parameters of $FP(O)(N_3)_2$ and $FP(O)(NCO)_2$

parameters[a]	$FP(O)(N_3)_2$		$FP(O)(NCO)_2$		
	calculated[b]		calculated[b]		XRD[c]
	anti-syn	*syn-syn*	*anti-syn*	*syn-syn*	
r(P–O)	1.448	1.454	1.447	1.451	1.4465(18)
r(P–F)	1.557	1.549	1.556	1.553	1.5286(15)
r(P–N1)	1.679	1.671	1.650	1.644	1.6251(17)
r(P–N2)	1.671	1.678	1.639	1.644	1.6250(17)
r(N1–N3/C1)	1.234	1.233	1.211	1.209	1.210(2)
r(N2–N4/C2)	1.234	1.234	1.206	1.209	1.210(2)
r(N3–N5/C1–O1)	1.119	1.119	1.154	1.155	1.148(2)
r(N4–N6/C2–O2)	1.120	1.119	1.156	1.155	1.148(2)
∠(FPO)	116.6	116.3	115.0	114.8	112.44(10)
∠(OPN1)	117.8	118.4	117.2	117.4	117.22(7)
∠(OPN2)	112.9	116.5	115.0	117.4	117.22(7)
∠(N1PN2)	106.5	103.7	104.7	102.7	107.38(12)
∠(PN1N3/C1)	119.8	120.2	137.1	138.1	139.59(14)
∠(PN2N4/C2)	121.8	119.7	144.4	138.1	139.59(14)
∠(N1N3N5/C1O1)	174.1	173.7	175.2	175.2	173.06(19)
∠(N2N4N6/C2O2)	173.7	173.9	175.5	175.2	173.06(19)
ϕ(OP–N1N3/C1)	18.3	32.6	3.0	–5.8	54.8(2)
ϕ(OP–N2N4/C2)	178.3	10.1	176.7	5.8	–54.8(2)

[a] Bond lengths and angles are given in [Å] and [deg], respectively. For labeling of atoms, see Figure 1. [b] Calculated results at the B3LYP/6-311+G(3df) level of theory. [c] Experimental results of $FP(O)(NCO)_2$ determined by X-ray crystallography (XRD).

Computationally, the main differences between the azide and isocyanate are the angles at the bridging nitrogen atoms. Much smaller angles were predicted for the azide (*anti-syn*: ∠(PN1N3) = 119.8º, ∠(PN2N4) = 121.8º, *syn-syn*: ∠(PN1N3) = 120.2º) than those for the isocyanates (*anti-syn*: ∠(PN1C1) = 137.1º, ∠(PN2C2) = 144.4º, *syn-syn*: ∠(PN1C1) = 138.1º). Interestingly, for both molecules, the P=O bonds are longer while the P–F bonds are shorter in the *syn-syn* conformers than those in the *anti-syn* ones. Similar conformation-dependent changes in bond length have been theoretically explored for the closely related molecules $F_2P(O)N_3$ and $F_2P(O)NCO$,[25] for which the $n_\sigma(N_\alpha) \rightarrow \sigma^*(P{=}O)$ hyperconjugation interactions have been suggested. The diisocyantate displays a highly distorted tetrahedral geometry at the central phosphorus atom, with bond angles varying from 99.96(7)º (∠(F1P1N1)) to 117.22(7)º (∠(O2P1N1)). The P=O bond length in $FP(O)(NCO)_2$ is 1.4465(18) Å, which is longer than that in $F_2P(O)NCO$ (1.4377(19) Å),[25] consistent with a less positive phosphorus atom in the former molecule. Similarly, the P–F bond is weakened and its length in $FP(O)(NCO)_2$ (1.5286(15) Å) is much longer than those in $F_2P(O)NCO$ (1.5166(17) and 1.5195(18) Å).[25] The angles at the bridging nitrogen atom in the diisocyanate is 139.59(14)º, wider than that in $F_2P(O)NCO$ (132.5(2)º), this is probably due to the repulsive interactions between the two NCO moieties.

Consistent with the red-shift for the P=O stretching vibration frequencies from the gas phase (1344 cm^{-1}, IR) to the solid state (1301 cm^{-1}, Raman), the packing diagram for $FP(O)(NCO)_2$ (Figure 6) exhibits intermolecular interactions with short O(2)···C(1) distance of 2.901(2) Å, which is comparable with the similar intermolecular O(2)···C(1) contact through a distance of 2.875 Å.[36] Both distances are much shorter than the sum of the van der Waals radii of oxygen (1.52 Å) and carbon (1.70 Å).[76]

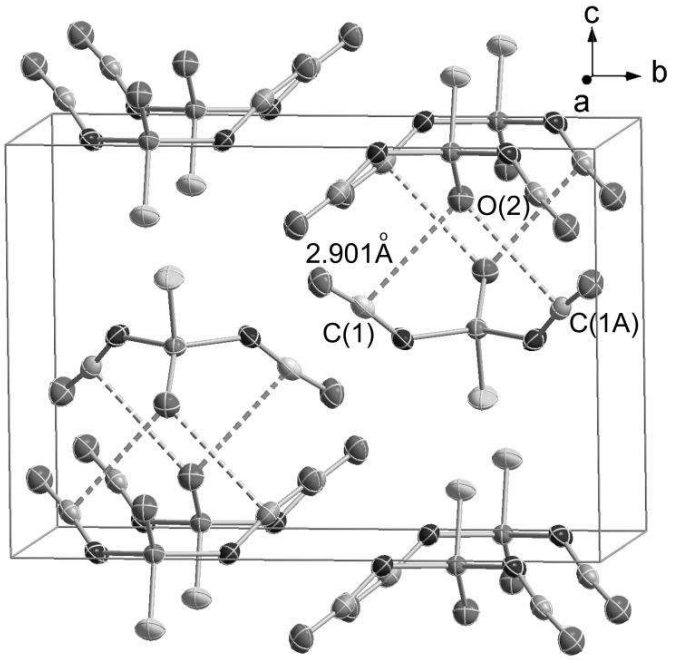

Figure 6. View along the *a*-axis of the unit cell of $FP(O)(NCO)_2$ showing the intermolecular O(2)···C(1) bridges.

Conclusions

Two structurally related fluorophosphoryl pseudohalides $FP(O)(N_3)_2$ and $FP(O)(NCO)_2$ have been synthesized and fully characterized with IR, Raman, and NMR spectroscopy. In line with the CCSD(T)/aug-cc-pVTZ//B3LYP/6-311+G(3df) computed energy differences of 3.8 and 3.2 kJ mol^{-1} between the *syn-syn* and *syn-anti* conformers for $FP(O)(N_3)_2$ and $FP(O)(NCO)_2$, the vibrational spectra of the two monofluorinated compounds demonstrate the dominant composition of the lower-energy *syn-syn* conformers for both compounds, and the higher-energy *syn-anti* conformers have estimated abundances of 16.6% and 29.1% for the azide and isocyanate, respectively. In the solid state, the X-ray crystallographic structure of diisocyanate $FP(O)(NCO)_2$ shows a C_s symmetry with the two NCO ligands in *syn*-conformation to the P=O bonds with a dihedral angle of 54.80(15)º.

Declaration of Competing Interest

The authors report no declarations of interest.

Appendix A. Supplementary data

Supplementary material related to this article can be found, in the online version, at doi:

Acknowledgements

This work was supported by the National Natural Science Foundation of China (21673147). We gratefully acknowledge Prof. H. Willner for his generous support.

References:

[1] S. Bräse, C. Gil, K. Knepper, V. Zimmermann, Organic azides: an exploding diversity of a unique class of compounds, Angew. Chem. Int. Ed. 44 (2005) 5188–5240.

[2] C. Knapp, J. Passmore, On the way to "solid nitrogen" at normal temperature and pressure? Binary azides of heavier group 15 and 16 elements, Angew. Chem. Int. Ed. 43 (2004) 4834–4836.

[3] I.C. Tornieporth-Oetting, T.M. Klapötke, Covalent inorganic azides, Angew. Chem. Int. Ed. 34 (1995) 511–520.

[4] P. Portius, A.C. Filippou, G. Schnakenburg, M. Davis, K.-D. Wehrstedt, Neutral lewis base adducts of silicon tetraazide, Angew. Chem. Int. Ed. 49 (2010) 8013–8016.

[5] X.Q. Zeng, M. Gerken, H. Beckers, H. Willner, Synthesis and characterization of carbonyl diazide, $OC(N_3)_2$, Inorg. Chem. 49 (2010) 9694–9699.

[6] K. Banert, Y.-H. Joo, T. Rüffer, B. Walfort, H. Lang, The exciting chemistry of tetraazidomethane, Angew. Chem. Int. Ed. 46 (2007) 1168–1171.

[7] S. Schulz, B. Lyhs, G. Jansen, D. Bläser, C. Wölper, Syntheses and structures of triazides of heavy group 15 elements, Chem. Commun. 47 (2011) 3401–3403.

[8] A. Schulz, A. Villinger, Mono- and diazides of bismuth, Organometallics 30 (2011) 284–289.

[9] M. Goebel, K. Karaghiosoff, T.M. Klapötke, The first structural characterization of a binary P–N molecule: the highly energetic compound P_3N_{21}, Angew. Chem. Int. Ed. 45 (2006) 6037–6040.

[10] R. Haiges, J.A. Boatz, A. Vij, V. Vij, M. Gerken, S. Schneider, T. Schroer, M. Yousufuddin, K.O. Christe, Polyazide chemistry: preparation and characterization of $As(N_3)_5$, $Sb(N_3)_5$, and $[P(C_6H_5)_4][Sb(N_3)_6]$, Angew. Chem. Int. Ed. 43 (2004) 6676–6680.

[11] X.Q. Zeng, H. Beckers, E. Bernhardt, H. Willner, Synthesis and characterization of sulfuryl diazide, $O_2S(N_3)_2$, Inorg. Chem. 50 (2011) 8679–8684.

[12] T.M. Klapötke, B. Krumm, M. Scherr, R. Haiges, K.O. Christe, The binary selenium(IV) azides $Se(N_3)_4$, $[Se(N_3)_5]^-$, and $[Se(N_3)_6]^{2-}$, Angew. Chem. Int. Ed. 46 (2007) 8686–8690.

[13] T.M. Klapötke, B. Krumm, M. Scherr, Studies on the properties of organoselenium(IV) fluorides and azides, Inorg. Chem. 47 (2008) 4712–4722.

[14] R. Haiges, J.A. Boatz, A. Vij, M. Gerken, S. Schneider, T. Schroer, K.O. Christe, Polyazide Chemistry: preparation and characterization of $Te(N_3)_4$ and $[P(C_6H_5)_4]_2[Te(N_3)_6]$ and evidence for $[N(CH_3)_4][Te(N_3)_5]$, Angew. Chem. Int. Ed. 2003, 42, 5847–5851.

[15] T.M. Klapötke, B. Krumm, K. Polborn, Isolation of a stable covalent selenium azide $RSeN_3$, J. Am. Chem. Soc. 126 (2004) 710–711.

[16] T.M. Klapötke, B. Krumm, P. Mayer, I. Schwab, Binary tellurium(IV) azides: $Te(N_3)_4$ and $[Te(N_3)_5]^-$, Angew. Chem. Int. Ed. 42 (2003) 5843–5846.

[17] P. Portius, P.W. Fowler, H. Adams, T.Z. Todorova, Experimental and theoretical

characterization of the hexaazidophosphate(V) ion, Inorg. Chem. 47 (2008) 12004–12009.

[18]X.Q. Zeng, H. Beckers, H. Willner, R.J.F. Berger, S.A. Hayes, N.W. Mitzel, Structure and conformational properties of azido(difluoro)phosphane, F_2PN_3, Eur. J. Inorg. Chem. 2011 (2011) 895–905.

[19]X.Q. Zeng, H. Beckers, H. Willner, Difluoro- λ^5- phosphinonitrile $F_2P{\equiv}N$: matrix isolation and photoisomerization into $FP{=}NF$, Angew. Chem. Int. Ed. 48 (2009) 4828–4831.

[20]X.X. Chu, Y. Yang, B. Lu, Z. Wu, W.Y. Qian, C. Song, X.F. Xu, M. Abe, X.Q. Zeng, Methoxyphosphinidene and isomeric methylphosphinidene oxide, J. Am. Chem. Soc. 140 (2018) 13604–13608.

[21]W.W. Wilson, A.J. Clough, R. Haiges, M. Rahm, K.O. Christe, Syntheses of diphenylaminodiazidophosphane and diphenylaminofluoroazidophosphane, Inorg. Chem. 54 (2015) 11859–11867.

[22]F. Dielmann, O. Back, M. Henry-Ellinger, P. Jerabek, G. Frenking, G. Bertrand, A crystalline singlet phosphinonitrene: a nitrogen atom–transfer agent, Science 337 (2012) 1526–1528.

[23]A. Schulz, A. Villinger, Stabilized transient R_2PN species, Angew. Chem. Int. Ed. 52 (2013) 3068–3070.

[24]A.V. Akimov, Y.S. Ganushevich, D.V. Korchagin, V.A. Miluykov, E.Y. Misochko, The EPR spectrum of triplet mesitylphosphinidene: reassignment and new assignment, Angew. Chem. Int. Ed. 56 (2017) 7944–7947.

[25]X.Q. Zeng, M. Gerken, H. Beckers, H. Willner, Spectroscopic and structural studies of difluorophosphoryl azide $F_2P(O)N_3$, difluorophosphoryl isocyanate $F_2P(O)NCO$, and difluorophosphoric acid anhydride, $F_2(O)POP(O)F_2$, Inorg. Chem. 49 (2010) 3002–3010.

[26]Z. Wu, H.M. Li, B.F. Zhu, X.Q. Zeng, S.A. Hayes, N.W. Mitzel, H. Beckers, R.J.F. Berger, Conformational composition, molecular structure and decomposition of difluorophosphoryl azide in the gas phase, Phys. Chem. Chem. Phys. 17 (2015) 8784–8791.

[27]X.Q. Zeng, H. Beckers, H. Willner, P. Neuhaus, D. Grote, W. Sander, Difluorophosphoryl nitrene $F_2P(O)N$: matrix isolation and unexpected rearrangement to F_2PNO, Chem. Eur. J. 15 (2009) 13466–13473.

[28]S. Vyas , S. Muthukrishnan , J. Kubicki , R.D. McCulla , G. Burdzinski , M. Sliwa , M.S. Platz, C.M. Hadad, Ultrafast spectroscopy and computational study of the photochemistry of diphenylphosphoryl azide: direct spectroscopic observation of a singlet phosphorylnitrene, J. Am. Chem. Soc. 132 (2010) 16796–16804.

[29]R.D. McCulla, G.A. Gohar, C.M. Hadad, M.S. Platz, Computational study of the curtius-like rearrangements of phosphoryl, phosphinyl, and phosphinoyl azides and their corresponding nitrenes, J. Org. Chem. 72 (2007) 9426–9438.

[30]X.X. Chu, C. Song, Y. Yang, X.Q. Zeng, Oxidation of a phosphinidene oxide: formation of a dioxaphosphirane oxide with oxygen scrambling, Chem. Commun. 55 (2019) 245–248.

[31]A. Mardyukov, F. Keul, P.R. Schreiner, Isolation and characterization of the free phenylphosphinidene chalcogenides $C_6H_5P{=}O$ and $C_6H_5P{=}S$, the phosphorous analogues of nitrosobenzene and thionitrosobenzene, Angew. Chem. Int. Ed. 59 (2020) 12445–12449.

[32]M. Alonso, M.E. García, M.A. Ruiz, H. Hamidov, J.C. Jeffery, Chemistry of the phosphinidene oxide ligand, J. Am. Chem. Soc. 126 (2004) 13610–13611.

[33]J.H. Werner, T.A. Cool, Flame sampling photoionization mass spectrometry of CH_3PO_2 and

CH_3OPO_2, Chem. Phys. Lett. 275 (1997) 278–282.

[34]X.Q. Zeng, H. Beckers, H. Willner, Elusive O═P≡N, a rare example of phosphorus $\sigma^2\lambda^5$-coordination, J. Am. Chem. Soc. 133 (2011) 20696–20699.

[35]Z. Wu, C. Song, J. Liu, B. Lu, Y. Lu, T. Trabelsi, J.S. Francisco, X.Q. Zeng, Photochemistry of OPN: formation of cyclic PON and reversible combination with carbon monoxide, Chem. Eur. J. 24 (2018) 14627–14630.

[36]X.Q. Zeng, E. Bernhardt, H. Beckers, H. Willner, Synthesis and characterization of the phosphorus triazides $OP(N_3)_3$ and $SP(N_3)_3$, Inorg. Chem. 50 (2011) 11235–11241.

[37]Y.Y. Qin, B. Lu, G. Rauhut, M. Hagedorn, K. Banert, C. Song, X. Chu, L. Wang, X.Q. Zeng, The simplest, isolable, alkynyl isocyanate HC≡CNCO: synthesis and characterization, Angew. Chem. Int. Ed. 58 (2019) 17277–17281.

[38]V.A. Peshkov, O.P. Pereshivko, A.A. Nechaev, A.A. Peshkov, E.V. Van der Eycken, Reactions of secondary propargylamines with heteroallenes for the synthesis of diverse heterocycles, Chem. Soc. Rev. 47 (2018) 3861–3898.

[39]E. Delebecq, J.-P. Pascault, B. Boutevin, F. Ganachaud, On the versatility of urethane/urea bonds: reversibility, blocked isocyanate, and non-isocyanate polyurethane, Chem. Rev. 113 (2013) 80–118.

[40]T.M. Klapötke, B. Krumm, S. Rest, R. Scharf, J. Schwabedissen, H.-G. Stammler, N.W. Mitzel, Carbonyl diisocyanate $CO(NCO)_2$: synthesis and structures in solid state and gas phase, J. Phys. Chem. A 120 (2016) 4534–4541.

[41]Q.F. Liu, H.M. Li, Z. Wu, D.Q. Li, H. Beckers, G. Rauhut, X.Q. Zeng, Photolysis of carbonyl diisocyanate: generation of isocyanatocarbonyl nitrene and diazomethanone, Chem. Asian J. 11 (2016) 2953–2959.

[42]A.M. Nolan, B.K. Amberger, B.J. Esselman, V.S. Thimmakondu, J.F. Stanton, R.C. Woods, R.J. McMahon, Carbonyl diazide, $OC(N_3)_2$: synthesis, purification, and IR spectrum, Inorg. Chem. 51 (2012) 9846–9851.

[43]X.Q. Zeng, H. Beckers, H. Willner, Matrix isolation of two isomers of N_4CO. Angew. Chem. Int. Ed. 50 (2011) 482–485.

[44]G. Maier, M. Naumann, H.P. Reisenauer, J. Eckwert, Diisocyanate, Angew. Chem. Int. Ed. Engl. 35 (1996) 1696–1697.

[45]A. Schulz, T.M. Klapötke, Does diisooxocyan (OCN−NCO) exist?, Inorg. Chem. 35 (1996) 4791–4793.

[46]G. de Petris, F. Cacace, R. Cipollini, A. Cartoni, M. Rosi, A. Troiani, Experimental detection of theoretically predicted N_2CO, Angew. Chem. Int. Ed. 44 (2005) 462–465.

[47]Bo Lu, Y.Y. Qin, C. Song, W.Y. Qian, L.N. Wang, X.Q. Zeng, O_2-oxidation of cyanomethylene radical: infrared identification of Criegee intermediates *syn*- and *anti*-NCC(H)OO, Chin. J. Chem. Phys. 33 (2020) 151–159.

[48]G. Maier, H.P. Reisenauer, K. Rademacher, Cyanocarbene, isocyanocarbene, and azacyclopropenylidene: a matrix-spectroscopic study, Chem. Eur. J. 4 (1998) 1957–1963.

[49]K. Banert, R. Arnold, M. Hagedorn, P. Thoss, A.A. Auer, 1-azido-1-alkynes: synthesis and spectroscopic characterization of azidoacetylene, Angew. Chem. Int. Ed. 51 (2012) 7515–7518.

[50]Y. Zhu, N.S Hosmane, Liquid- phase synthesis of boron isocyanates: precursors to boron nanoparticles, Angew. Chem. Int. Ed. 57 (2018) 14888–14890.

[51]C.L. Schmidt, M. Jansen, Crystal structure and dimorphism of silicon tetraisocyanate $Si(NCO)_4$, Z. Anorg. Allg. Chem. 638 (2012) 275–278.

[52]W.G. Wang, M.F. Ge, L. Yao, X.Q. Zeng, Z. Sun, D.X. Wang, Gas-phase spectroscopy of the unstable sulfur diisocyanate molecule $S(NCO)_2$, ChemPhysChem 7 (2006) 1382–1387.

[53]G.S. Forbes, H.H. Anderson, Cyanates of silicon, phosphorus and boron. Instability of certain ternary boron compounds, J. Am. Chem. Soc. 62 (1940) 761–763.

[54]G.G. Flaskerud, K.E. Pullen, J.M. Shreeve, Reactions of halodifluorophosphines with silver salts, Inorg. Chem. 8 (1969) 728–730.

[55]D.Q. Li, J. Schwabedissen, H.-G. Stammler, N. W. Mitzel, H. Willner, X.Q. Zeng, Dichlorophosphanyl isocyanate – spectroscopy, conformation and molecular structure in the gas phase and the solid state, Phys. Chem. Chem. Phys. 18 (2016) 26245–26253.

[56]J. Schwabedissen, P.C. Trapp, H.-G. Stammler, N.W. Mitzel, Z. Wu, X.X. Chu, X.Q. Zeng, Spectroscopic properties, conformation and structure of difluorothiophosphoryl isocyanate in the gaseous and solid phase, ChemistryOpen 9 (2020) 913–920.

[57]F.A. Miller, W.K. Baer, The infrared, Raman and ultraviolet spectra of $P(NCO)_3$ and $PO(NCO)_3$, Spectrochim. Acta A 18 (1962) 1311–1323.

[58]S.R. O'Neill, J.M. Shreeve, Fluorophosphorus azides, Inorg. Chem. 11 (1972) 1629–1631.

[59]P. Rovnaník, Z. Žák, M. Černík, Syntheses of phosphoryl chloro- and bromofluorides and crystal structures of $POFCl_2$ and POF_2Cl, Z. Anorg. Allg. Chem. 632 (2006) 1356–1362.

[60]CrysAlisPro, Version 1.171.33.42, Oxford Diffraction Ltd.

[61]CrysAlisPro, Version 1.171.38.41, Rigaku Oxford Diffraction, 2015.

[62]G.M. Sheldrick, SHELXT – Integrated Space-Group and Crystal-Structure Determination. Acta Crystallogr. A 71 (2015) 3–8.

[63]G.M. Sheldrick, SHELXTL97, University of Göttingen, 2008.

[64]O.V. Dolomanov, L.J. Bourhis, R.J. Gildea, J.A.K. Howard, H. Puschmann, OLEX2 : A complete structure solution, refinement and analysis program. J. Appl. Crystallogr. 42 (2009) 339–341.

[65]A.D. Becke, Density-functional thermochemistry. III. The role of exact exchange, J. Chem. Phys. 98 (1993) 5648–5652.

[66]A.D. Becke, Density-functional exchange-energy approximation with correct asymptotic behavior, Phys. Rev. A 38 (1988), 3098–3100.

[67]C. Adamo, V. Barone, Exchange functionals with improved long-range behavior and adiabatic connection methods without adjustable parameters: the *m*PW and *m*PW1PW models, J. Chem. Phys. (108) 1998, 664.

[68]Gaussian 09, Revision D.01, M.J. Frisch, G.W. Trucks, H.B. Schlegel, G.E. Scuseria, M.A. Robb, J.R. Cheeseman, G. Scalmani, V. Barone, G.A. Petersson, H. Nakatsuji, X. Li, M. Caricato, A. Marenich, J. Bloino, B.G. Janesko, R. Gomperts, B. Mennucci, H.P. Hratchian, J.V. Ortiz, A.F. Izmaylov, J.L. Sonnenberg, D. Williams-Young, F. Ding, F. Lipparini, F. Egidi, J. Goings, B. Peng, A. Petrone, T. Henderson, D. Ranasinghe, V.G. Zakrzewski, J. Gao, N. Rega, G. Zheng, W. Liang, M. Hada, M. Ehara, K. Toyota, R. Fukuda, J. Hasegawa, M. Ishida,

T. Nakajima, Y. Honda, O. Kitao, H. Nakai, T. Vreven, K. Throssell, J.A. Montgomery, Jr., J.E. Peralta, F. Ogliaro, M. Bearpark, J.J. Heyd, E. Brothers, K.N. Kudin, V.N. Staroverov, T. Keith, R. Kobayashi, J. Normand, K. Raghavachari, A. Rendell, J.C. Burant, S.S. Iyengar, J. Tomasi, M. Cossi, J.M. Millam, M. Klene, C. Adamo, R. Cammi, J.W. Ochterski, R.L. Martin, K. Morokuma, O. Farkas, J.B. Foresman, D.J. Fox, Gaussian, Inc., Wallingford CT, (2016).

[69] K. Raghavachari, G.W. Trucks, J.A. Pople, M. Head-Gordon, A fifth-order perturbation comparison of electron correlation theories, Chem. Phys. Lett. 157 (1989) 479–483.

[70] H.J. Werner, P.J. Knowles, G. Knizia, F.R. Manby, M. Schütz, Molpro: a general-purpose quantum chemistry program, WIRES. Comput. Mol. Sci. 2 (2012) 242−253.

[71] X.Q. Zeng, W.G. Wang, F.Y. Liu, M.F. Ge, Z. Sun, D.X. Wang, Electronic structure of binary phosphoric and arsenic triazides, Eur. J. Inorg. Chem. 2006 (2006) 416–421.

[72] R. Haiges, A. Vij, J.A. Boatz, S. Schneider, T. Schroer , M. Gerken, K.O. Christe, First structural characterization of binary As^{III} and Sb^{III} azides, Chem. Eur. J. 10 (2004) 508–517.

[73] E.A. Ruben, J.A. Plumley, M.S. Chapman, J.D. Evanseck, Anomeric effect in “high energy” phosphate bonds. Selective destabilization of the scissile bond and modulation of the exothermicity of hydrolysis, J. Am. Chem. Soc. 130 (2008), 3349−3358.

[74] G. Lowe, G.R.J. Thatcher, J.C.G. Turner, A. Waller, D.J. Watkin, Stereoelectronic effects in sulfate diesters and sulfuric acid, J. Am. Chem. Soc. 110 (1988) 8512–8520.

[75] N. Erdeljac, C. Mück-Lichtenfeld, C.G. Daniliuc, R. Gilmour, Conformational analysis of acyclic α-fluoro sulfur motifs, Chem. Eur. J. (2020) https://doi.org/10.1002/chem.202003361.

[76] A. Bondi, van der Waals volumes and radii, J. Phys. Chem. 68 (1964) 441–451.